

The FIRST Sample of Ultraluminous Infrared Galaxies at High Redshift I. Sample and Near-IR Morphologies

S.A. Stanford¹

Physics Department, University of California at Davis, and the Institute of Geophysics and Planetary Physics, Lawrence Livermore National Laboratories, Livermore, CA, 94550;

adam@igpp.ucllnl.org

Daniel Stern^{1,2}

Department of Astronomy, University of California, Berkeley, CA 94720;

dan@bigz.berkeley.edu

Wil van Breugel

Institute of Geophysics and Planetary Physics, Lawrence Livermore National Laboratories, Livermore, CA, 94550; wil@igpp.ucllnl.org

Carlos De Breuck

Leiden Observatory, and Institute of Geophysics and Planetary Physics, Lawrence Livermore National Laboratories, Livermore, CA, 94550; debreuck@igpp.ucllnl.org

Received _____; accepted _____

¹Visiting Astronomer, Infrared Telescope Facility, University of Hawaii, NASA

²current address: Jet Propulsion Laboratory, California Institute of Technology, Mail Stop 169-327, Pasadena, CA 91109

ABSTRACT

We present a new sample of distant ultraluminous infrared galaxies. The sample was selected from a positional cross-correlation of the *IRAS* Faint Source Catalog with the FIRST database. Objects from this set were selected for spectroscopy by virtue of following the well-known star-forming galaxy correlation between 1.4 GHz and 60 μ m flux, and by being optically faint on the POSS. Optical identification and spectroscopy were obtained for 108 targets at the Lick Observatory 3 m telescope. Most objects show spectra typical of starburst galaxies, and do not show the high ionization lines of active galactic nuclei. The redshift distribution covers $0.1 < z < 0.9$, with 13 objects at $z > 0.5$ and an average redshift of $\bar{z} = 0.31$. *K*-band images were obtained at the IRTF, Lick, and Keck observatories in sub-arcsec seeing of all optically identified targets. About 2/3 of the objects appear to be interacting galaxies, while the other 1/3 appear to be normal. Nearly all the identified objects have far-IR luminosities greater than $10^{11}L_{\odot}$, and $\sim 25\%$ have $L_{FIR} > 10^{12}L_{\odot}$.

Subject headings: galaxies: starburst — galaxies: interactions — infrared: galaxies — radio continuum: galaxies

1. Introduction

Observations by the Infrared Astronomy Satellite (*IRAS*) led to the discovery of a class of galaxies with enormous far-IR luminosities. Subsequent observations over a large range of wavelengths have shown that these objects, called ULIG for ultraluminous infrared galaxies, have 1) bolometric luminosities and space densities comparable to those of optical quasars (Sanders et al. 1988); 2) a broad range in host galaxy spectral type, including starburst galaxies, Seyfert I and II, radio galaxies, and quasars; 3) morphologies often suggestive of recent interactions or merging (Carico et al. 1990; Leech et al. 1994; Rigopoulou et al. 1999); and 4) large amounts of molecular gas concentrated in small (<1 kpc) central regions (e.g. Scoville et al. 1989; Solomon et al. 1997). Understanding the nature of the prime energy source in ULIG has proven difficult (e.g. Smith, Lonsdale, & Lonsdale 1998). Many of the observed characteristics indicate that very strong starbursts could be the culprit. Alternatively, an active galactic nucleus (AGN) may power the ULIG (e.g. Lonsdale, Smith, & Lonsdale 1993). The very high luminosities suggest an evolutionary connection between ULIG and quasars, wherein a dust-enshrouded central massive black hole is gradually revealed as the appearance of the object changes from ULIG to quasar (Sanders et al. 1988).

Much effort has been expended in trying to determine the primary source of energy—starbursts or AGN—driving the large FIR luminosities. The recent studies using ISO indicate that the vast majority of the power comes from starbursts in $\sim 80\%$ of the observed systems (Genzel et al. 1998; Lutz et al. 1998). Rigopoulou et al. (1999) present the results of an expanded version of the mid-IR spectroscopic survey first reported by Genzel et al. (1998). Using ISO to observe 62 ULIG at $z < 0.3$, they measured the line to continuum ratio of the $7.7 \mu\text{m}$ polycyclic aromatic hydrocarbon (PAH) feature to differentiate between starburst and AGN as the dominant source of the large FIR luminosity. PAH features have been shown to be strong in starburst galaxies and weak in AGN (Moorwood 1986; Roche

et al. 1991). Rigopoulou et al. confirmed the results of Genzel et al. (1998), and also found, based on near-IR imaging, that approximately 2/3 of their sample have double nuclei and nearly all the objects show signs of interactions. For a recent review of ULIG see Sanders & Mirabel (1996).

ULIG are also of great interest for studies of early star formation in the building of galaxies. Recent sub-mm observations suggest that objects similar to ULIG may contain a significant fraction of the star formation at high redshifts (e.g. Lilly et al. 1999). But so far most studies have found ULIG only in the nearby universe. Sanders et al. (1988) initially studied a group of 10 objects at $z < 0.1$. Previously published systematic surveys have found objects mostly at $z < 0.4$ (Leech et al. 1994; Clements et al. 1996a, 1996b). A few high redshifts objects have been found, all of which turn out to contain hidden AGN. These include FSC 15307+3252 at $z = 0.926$ (Cutri et al. 1994) and FSC 10214+4724 at $z = 2.286$ (Rowan-Robinson et al. 1991). The former object was found to exhibit a highly polarized continuum, indicating the presence of a buried quasar (Hines et al. 1995) while the latter was found to be lensed (Eisenhardt et al. 1996) and also shows signs of containing a hidden AGN (Lawrence et al. 1993; Elston et al. 1994; Goodrich et al. 1996). Further progress in this field has been hampered by the lack of identified ULIG at moderately high redshifts.

No new deep far-IR survey will become available prior to the launch of *SIRTF*, which will be capable of studying ULIG in detail at high redshifts. So, the *IRAS* database remains the primary source of targets for finding high redshift ULIG. Radio observations provide a relatively unbiased method for extracting FIR galaxies from the *IRAS* Faint Source Catalog (FSC; Moshir et al. 1992) because radio continuum emission is relatively unaffected by extinction in dense gas and dust. Such FIR/radio samples are ideal for detailed investigations of the complex relationships between the interstellar media, starbursts, and possible AGN in ULIG. For example, a sample of radio-loud objects was constructed by

cross-correlating the *IRAS* FSC with the Texas 365 MHz radio catalog (TXFS; Dey & van Breugel 1990). Subsequent optical identifications and spectroscopy showed that the TXFS objects tend to be distant AGN. So a radio-quiet sample, extracted from the FSC, should be an excellent means of finding ULIG without AGN—i.e. powered by starbursts—at interesting cosmological distances. In this paper, we report on such a sample: we describe the sample selection process and discuss the near-IR imaging. We defer a detailed analysis of the radio properties and optical spectroscopy to future papers.

2. The FIRST/FSC Sample

We have used two large area surveys in the radio and far-IR, which we briefly describe here, to select ULIG candidates. In the radio, we have used the FIRST (Faint Images of the Radio Sky at Twenty cm; Becker, White, & Helfand 1995). Using the VLA, this project is surveying π steradians down to a 5σ limit of 1 mJy with 5 arcsec resolution and subarcsec positional accuracy. One of the problems with finding distant ULIG using *IRAS* is that there are many faint galaxies visible in a deep optical image within the relatively large error ellipse of an FIR source. The high resolution and good positional information of FIRST offer an excellent means of choosing the best of the many optical candidates on which to spend valuable large telescope time getting redshifts. We used the second version of the catalog (released 1995 October 16), which samples 2925 degrees² in two regions of sky in the North ($7^h20^m < \text{RA}(\text{J2000}) < 17^h20^m$, $22^\circ2 < \text{Dec}(\text{J2000}) < 42^\circ5$) and South ($21^h20^m < \text{RA}(\text{J2000}) < 3^h20^m$, $-2^\circ5 < \text{Dec}(\text{J2000}) < 1^\circ6$) Galactic Caps. In the far-IR we have used the *IRAS* FSC (Moshir et al. 1992) which resulted from the Faint Source Survey (FSS). Relative to the *IRAS* Point Source Catalog, the FSS achieved better sensitivity by point-source filtering the detector data streams and then coadding those data before finding sources. At 60 μm (the band used for defining our candidates), the FSC covers the sky at

$|b| \gtrsim 10^{\circ}0$ and has a reliability (integrated over all signal-to-noise ratios) of $\gtrsim 94\%$. The limiting $60 \mu\text{m}$ flux density of the FSC is approximately 0.2 Jy, where the signal-to-noise ratio (SNR) is ~ 5 . The FSS also resulted in the Faint Source Reject file which contains extracted sources not in the FSC with an SNR above 3.0. We used the FSR, in addition to the FSC, with part of FIRST to increase the number of targets in the fall sky.

The *IRAS* FSC was positionally cross-correlated with the second version of the FIRST catalog, with the requirements that an FSC source must have a real $60 \mu\text{m}$ detection ($f_{\text{qual}} \geq 1$) and that it be within 60 arcsec of the FIRST source. The $60 \mu\text{m}$ band was chosen because it is more reliable than the $100 \mu\text{m}$ band and samples close to the wavelength peak of the ULIG power. The resulting FIRST-FSC (FF) catalog contains 2328 matches. To increase the available objects in the fall sky, we also performed a positional match of the FSR with the South Galactic Cap portion of FIRST, which yielded an additional 176 matches. The 20 cm and $60 \mu\text{m}$ flux densities for this sample of 2504 sources are plotted in Figure 1. The majority of the FF sources fall along the well-known radio-FIR correlation (Condon et al. 1991), extending from nearby starburst galaxies to much fainter FIR/radio flux levels. The surface density of such objects is approximately 1 degree^{-2} down to the $\sim 5\sigma$ limits of 1 mJy at 20 cm and ~ 0.2 Jy at $60 \mu\text{m}$.

We generated optical finding charts using the Digitized Sky Surveys, available from the Space Telescope Science Institute, for all 2504 matches. The radio source position and the FSC error ellipse were overlaid on these charts. Visual inspection of these finding charts was carried out to select optically faint targets for further study, with the expectation that such targets would be distant ULIG. Approximately 150 targets, which will carry the designation FF along with the usual coordinate naming scheme, were selected in this manner. A strict cutoff in optical magnitude was not employed, and we make no attempt to construct a sample which has a well-defined limiting magnitude in the optical. In practice,

the magnitude of the targets selected for optical imaging and spectroscopy depended on the observing conditions, i.e. some targets which are not visually faint on the DSS image were observed during cloudy conditions. While the FIRST and FSC catalogs do have well-defined flux limits, our sample was not constructed in order to be complete to a chosen flux level in either the radio nor the far-IR bands. The main goal of the survey is simply to find high-redshift ULIG. It is worth noting that our target list would include objects with observed characteristics in the radio, optical, and far-IR similar to those of FSC10214+4724 (which itself lies outside of the FIRST area that we used and so cannot fall into our catalog). We have not found any ULIG at redshifts as great as that of FSC10214+4724 in the ~ 3000 degree² surveyed.

3. Observations

During several runs from March 1996 to April 1999, the Kast spectrograph (Miller & Stone 1994) at the Shane 3 m telescope of Lick Observatory was used to obtain optical images and spectroscopy of the candidate ULIG from our FF catalog. The observing procedure typically consisted of taking two 300 s images in the r_S band, identifying the optical counterpart of the FF source in these data, and immediately following up with slit spectroscopy of the optical object. Because the resolution and positional accuracy of FIRST are high, it was usually clear which optical object coincided with the radio source. The FWHM of the seeing in the images was usually in the range 1.5–2.0 arcsec. Standard stars were observed in imaging mode when conditions were photometric. However, because much of the data were obtained during non-photometric conditions, r_S magnitudes will not be presented here for the sample. Unless the source morphology demanded a particular value, the position angle of the slit was set to the parallactic angle. The object was dithered along the slit by ~ 10 arcsec between two exposures to aid in fringe subtraction. Optical spectra

of 1200-6000s duration were obtained of the optical source using the 300 line mm^{-1} grating in the red-side spectrograph, which provides $\sim 4.6 \text{ \AA pixel}^{-1}$ resolution from 5070–10590 \AA , and a 452/3306 grism in the blue-side spectrograph which provides $\sim 2.5 \text{ \AA pixel}^{-1}$ resolution from 3000–5900 \AA . The slit width was set at 2 arcsec. The images and spectra were reduced using standard techniques.

Near-infrared images were obtained of the targets for which redshifts had been determined in order to better ascertain the morphologies of the galaxies. K' images were obtained for nearly all identified targets with NSFCAM at the IRTF 3 m telescope in 1998 August and 1999 February. Additional observations of 3 targets were obtained in service mode in September 1999. NSFCAM was used in its $0.3 \text{ arcsec pixel}^{-1}$ mode which provides a 77×77 arcsec field. Typical total exposure times per object were 960s; more distant objects were observed for twice this period. Conditions were photometric with seeing averaging 0.9 arcsec. Observations of standard stars from the Persson et al. (1998) list were obtained and used to calibrate the images onto the California Institute of Technology (CIT) system, which is defined in Elias et al. (1982). The data were reduced using standard techniques.

Five targets were observed in the K band using Gemini (McLean et al. 1993) at the Shane 3 m telescope on 1998 October 7. Gemini has $0.68 \text{ arcsec pixels}$ which give it a 174 arcsec field. Objects were observed for 1080 s each in photometric conditions with seeing of $\sim 1.2 \text{ arcsec}$. The data were reduced using standard techniques and calibrated onto the CIT system using observations of UKIRT faint source standards (Casali & Hawarden 1992).

Two distant targets were imaged at the Keck I telescope with NIRC (Matthews & Soifer 1994) in 1998 April. FF1106+3201 was observed in the K band for 16 minutes and FF1614+3234 was observed for 32 minutes in the K_s band. Both objects were observed in clear conditions with $\sim 0.5 \text{ arcsec}$ seeing. These data were reduced using standard

techniques and calibrated onto the CIT system using observations of UKIRT faint source standards (Casali & Hawarden 1992).

4. Results

4.1. Optical

We attempted spectroscopic observations of approximately 150 IRAS/FIRST candidates, of which 116 yielded redshift information. The 108 with infrared imaging are listed in Table 1; the 8 sources with redshifts but lacking infrared images are not considered further. The sources which did not provide useful spectra were usually observed in poor conditions; the reasons for their lack of redshifts were not because of having intrinsically challenging spectra. The object names in Table 1 are based on the FIRST radio position. The source in the FIRST catalog would have the name given by the object’s coordinates shown in our Table 1, in the format FIRST *Jhhmmss.s+ddmmss* where the coordinates are truncated, not rounded. In the *IRAS* FSC, the FIR source name is different from that implied by our FF name, so we have included the FSC source name as a column in Table 1. The Z designation in the FSC name means that the FIR source is from the FSR catalog.

The typical resolution of the spectroscopy was $\approx 15 \text{ \AA}$ (FWHM) at $\lambda > 5500 \text{ \AA}$, implying typical uncertainties of $\lesssim 0.002$ in redshift. Redshifts were determined from the spectra after identifying probable emission lines and continuum features. In practice the features most often used were the [O II] $\lambda 3727$, [O III] $\lambda 4959, 5007$, and H α lines, and the D4000 break. The vast majority of the spectra have the emission lines characteristic of star formation; very few show any signs, such as high ionization lines, of an AGN. Four sample spectra, covering a range in redshift, signal to noise, and spectral type, are shown in Figure 2. A more detailed analysis of the optical spectra is deferred to a later paper.

4.2. Near Infrared

The K' images are displayed for each object, along with the optical finding chart from the DSS, in Figure 3. Photometry of the FF objects was obtained from the K' images. In Table 1, the K magnitudes within 3 arcsec diameter apertures, centered on the peak of the near-IR emission, are given for each object. The 5σ detection limit in most of the images is $K \sim 19$ so the limiting factor in the uncertainty of the photometry is not the signal to noise, since most objects have magnitudes some 3–4 magnitudes brighter than the detection limit, but rather systematics in the zeropoint. We estimate that the uncertainty in the zeropoint is 0.03 mag. For most objects the 3 arcsec diameter aperture contains $\sim 70\%$ of the total light. The morphologies of the objects tend to show signs of galaxy interactions, including tidal tails, multiple nuclei, and disturbed outer envelopes. Approximately 2/3 of the sample show such features, while 1/3 of the sample appear to be normal galaxies. A brief description of the near-IR morphology for each FF is included in Table 1.

4.3. Radio

One of the major advantages of using FIRST in our survey is the high accuracy of its positional information. The coordinates listed in Table 1 are those of the radio source as given by the FIRST catalog, which has an absolute astrometric uncertainty of ~ 1 arcsec. The 20 cm VLA images of all objects listed in Table 1 were extracted from the FIRST database. The radio morphologies were classified by visual inspection of these cutout images, and by consulting the deconvolved sizes listed in the FIRST catalog. The 20 cm morphological information is given for each FF source in Table 1. The 20 cm flux densities listed in Table 1 have typical uncertainties of 10% at the 2 mJy level.

4.4. Far Infrared

Improved *IRAS* flux densities were obtained for all objects in Table 1 with the ADDSCAN utility at IPAC. In addition to the 60 μm band used to construct our FF catalog, data at 12 μm , 25 μm , and 100 μm was searched for detections. Almost none of the objects in Table 1 were detected at either of the shorter two wavelengths, so no information is included from these wavebands in Table 1. Many detections were obtained in the 100 μm data; these are included where available in Table 1, and one σ upper limits are indicated in parentheses. The uncertainty in the typical 60 μm measurement in the sample is $\sim 10\%$, and $\sim 15\%$ in the 100 μm band where detected. The 60 μm and 100 μm flux densities were used to calculate the far-infrared luminosity, as defined by Sanders & Mirabel (1996): $L(40\text{--}500 \mu\text{m}) = 4\pi D_L^2 C F_{FIR}[L_\odot]$, where D_L^2 is the luminosity distance in Mpc, $F_{FIR} = 1.26 \times 10^{-14}(2.58 \times f_{60} + f_{100})[Wm^{-2}]$, and $C = 1.6$. Throughout this paper we use $H_0 = 65 \text{ km s}^{-1} \text{ Mpc}^{-1}$ and $\Omega_M = 0.3$ with $\Lambda = 0$. When 100 μm detections could not be obtained with ADDSCAN, the 1σ limiting flux densities were used in the calculation of the L_{FIR} . The L_{FIR} are given in Table 1, and are plotted in Figure 4. The uncertainty in the L_{FIR} is dominated by a combination of the typical $\sim 10 - 15\%$ flux measurement errors and the $\sim 15\%$ uncertainty in the scaling factor C which accounts for the extrapolated flux longward of the 100 μm band.

5. Discussion

The reliability of the optical identification with the radio source for the objects in Table 1 is very high. The optical/radio source association with the FSC far-infrared source is less certain, because of the relatively large positional uncertainty of the *IRAS* detections. But there are at least four reasons to believe that the identified optical/radio sources are indeed the FSC sources as well. First, in all cases, the FIRST position is within twice the

1 σ error ellipse of the FSC source. Second, the optical spectra show emission lines typical of star-forming galaxies, as expected for most far-IR luminous objects. Third, in the cases where both 60 and 100 μm detections were obtained, the *IRAS* flux ratios are typical of FIR luminous galaxies (Soifer et al. 1987). Finally, in nearly all cases the FIR/radio flux ratio lies on the well-established correlation as seen in Figure 1.

There are at least two possible ways that the wrong association is being made. First, a galaxy optically brighter than the identified FF source could lie just outside the *IRAS* error ellipse and still be the source of the *IRAS* detection. But in our sample there are no such galaxies which are also detected by FIRST, as would be expected if such objects were the true source of the FIR emission. Second, a faint radio source could be missed by the FIRST survey that would coincide with the *FSC* source. Using the rms given in the FIRST catalog for each object, lower limits to the resulting $S_{60\mu\text{m}}/S_{20\text{cm}}$ ratios for objects beneath the *FIRST* detection limits are found to be $\sim 500\text{-}700$, far greater than the standard ratio for star-forming galaxies. Finally its worth noting that on average one expects to find only 0.035 FIRST sources within the typical *IRAS* error ellipse area, so the probability of a random radio source being associated with an FSC source is low. In our sample of 108 identified FF objects, approximately 4 could be due to radio sources unassociated with the far-IR source.

Although we defer the scientific analysis of the new sample to future contributions, we will briefly compare some basic global properties of our FF sample to those of other similarly large samples of high redshift ULIG which have been previously published, e.g. Leech et al. (1994) and Clements et al. (1996). Our new sample has ULIG at higher average redshift ($\bar{z} \sim 0.3$) than that of Leech et al. ($\bar{z} \sim 0.17$) and that of Clements et al. ($\bar{z} \sim 0.21$). As for the interaction rate, on which there has been some disagreement in the literature (Sanders & Mirabel 1996), our result that 2/3 of the sample shows signs of galaxy interactions is in

agreement with Leech et al. but not Clements et al., who found that $\sim 90\%$ of their sample were interacting systems. Finally, the rate of AGN-type optical spectra in our sample, which is only 10%, is somewhat less than the $\sim 25\%$ found by Clements et al. We do see a higher incidence of AGN-type spectra at the highest L_{FIR} as has been noted previously by several studies; for a review of this topic see Sanders & Mirabel (1996).

6. Summary

We have constructed a new survey of ULIG using a match of the *IRAS* FSC with the second version of the FIRST catalog, which covered nearly 3000 degrees². By choosing for further study only optically faint matches from the DSS which also fall on the radio-FIR flux correlation, we have attempted to find high redshift ULIG which are powered primarily by starbursts. Optical images and spectra were obtained of 108 such targets, which were found to lie in the redshift range $0.1 < z < 0.9$; a redshift histogram is shown in Figure 5. Nearly all of these targets have L_{FIR} greater than $10^{11}L_{\odot}$, and have a higher average redshift of $\bar{z} = 0.31$ than in other recent ULIG surveys. Near-IR imaging shows that while more than the majority of objects show clear signs of galaxy interactions, nearly 1/3 appear to be normal at arcsec resolution in the *K* band. With this sample, we intend to examine the nature of ULIG evolution in future contributions.

The authors thank the staff of Lick Observatory for their help in obtaining the optical data, and Bill Vacca and Dave Griep at the IRTF for their assistance in obtaining the near-IR data, and for conducting servicing observing for three of the sample objects. We have made use of the online facilities provided by IPAC. We also thank Bob Becker for providing us with the FIRST catalog and for help in using its contents. Finally we thank Rob Kennicutt for a speedy referee report. The Digitized Sky Surveys were produced at

the Space Telescope Science Institute under U.S. Government grant NAG-W-2166. The images of these surveys are based on photographic data obtained using the Oschin Schmidt Telescope on Palomar Mountain and the UK Schmidt Telescope. The plates were processed into the compressed digital form with permission of these institutions. The work by SAS, WvB, and CDB at IGPP/LLNL was performed under the auspices of the U.S. Department of Energy under contract W-7405-ENG-48 to the University of California. The work by DS was supported by IGPP grants 98-AP017 and 99-AP026.

REFERENCES

- Becker, R. White, R. & Helfand, D. 1995, ApJ, 450, 559
- Carico, D., Graham, J. R., Matthews, K., Wilson, T. D., Soifer, B. T., Neugebauer, G., & Sanders, D. B. 1990, ApJ, 349, L39
- Casali, M. & Hawarden, T. 1992, JCMT-UKIRT Newsletter, 4, 33
- Clements, D., Sutherland, W. J., Saunders, W., Efstathiou, G. P., McMahon, R. G., Maddox, S., Lawrence, A., & Rowan-Robinson, M. 1996a, MNRAS, 279, 459
- Clements, D., Sutherland, W. J., McMahon, R. G., & Saunders, W. 1996b, MNRAS, 279, 477
- Condon, J. J., Anderson, M. L., & Helou, G. 1991, ApJ, 378, 65
- Cutri, R. M., Huchra, J. P., Low, F. J., Brown, R. L., & vanden Bout, P. A. 1994, ApJ, 424, L65
- Dey, A. & van Breugel, W. 1990, IAU Colloquium 124, p. 309
- Eisenhardt, P. R., Armus, L, Hogg, D. W., Soifer, B. T., Neugebauer, G., & Werner, M. 1996, ApJ, 461, 72
- Elias, J.H., Frogel, J.A., Matthews, K., & Neugebauer, G. 1982, AJ, 87, 1029
- Elston, R., McCarthy, P. J., Eisenhardt, P., Dickinson, M., Spinrad, H., Januzzi, B. T., & Maloney, P. 1994, AJ, 107, 910
- Genzel, R. et al. 1998, ApJ, 498, 579
- Goodrich, R. W., Miller, J. S., Martel, A., Cohen, M. H., Tran, H. D., Ogle, P. M., & Vermeulen, R. C. 1996, ApJ, 456, L9
- Hines, D. C., Schmidt, G. D., Smith, P. S., Cutri, R. M., & Low, F. J. 1995, ApJ, 450, L1

- Kleinmann, S.G., Hamilton, D., Keel, W.C., Wynn-Williams, C.G., Eales, S.A., Becklin, E.E., & Kuntz, K.D. 1988, *ApJ*, 328, 161
- Lawrence, A., et al. 1993, *MNRAS*, 260, 281
- Leech, K.J., Rowan-Robinson, M., Lawrence, A., & Hughes, J. D. 1994, *MNRAS*, 267, 253
- Lilly, S.J., Eales, S.A., Gear, W.K.P., Hammer, F., Le Fevre, O., Crampton, D., Bond, J.R., & Dunne, L. 1999, *ApJ*, 518, 641
- Lonsdale, C., Smith, H., & Lonsdale, C. 1993, *ApJ*, 405, L9
- Lutz, D., Spoon, H. W. W., Rigopoulou, D., Moorwood, A. F. M., & Genzel, R. 1998, *ApJ*, 505, 103
- Matthews, K. & Soifer, B. T. 1994, *Experimental Astronomy*, 3, 77
- McLean, I.S. et al. *SPIE*, 1946, 513
- Miller, J.S. & Stone, R.P.S. 1994, *Lick Observatory Technical Reports # 66*
- Moorwood, A.F.M. 1986, *A&A*, 166, 4
- Moshir, M., Kopman, G., & Conrow, T. 1992, *IRAS Faint Source Survey, Explanatory Supplement, Version 2*
- Persson, S. E., Murphy, D. C., Krzeminski, W., Roth, M., & Rieke, M. J. 1998, *AJ*, 116
- Rigopoulou, D., Spoon, H.W.W., Genzel, R., Lutz, D., Moorwood, A.F.M., Tran, Q.D. 1999, *AJ*, 118, 2625
- Roche, P.F., Aitken, D.K., Smith, C.H., & Ward, M.J. 1991, *MNRAS*, 248, 606
- Rowan-Robinson, M. et al. 1991, *Nature*, 351, 719
- Sanders, D.B., Soifer, B. T., Elias, J. H., Madore, B. F., Matthews, K., Neugebauer, G., & Scoville, N. Z. 1988, *ApJ*, 325, 74
- Sanders, D. B. & Mirabel, I. F. 1996, *ARAA*, 34, 749

- Scoville, N. Z., Sanders, D. B., Sargent, A. I., Soifer, B. T., & Tinney, C. G. 1989, *ApJ*, 345, L25
- Smith, H.E., Lonsdale, C.J., & Lonsdale, C.J. 1998, *ApJ*, 492, 137
- Soifer, B.T., Sanders, D. B., Madore, B. F., Neugebauer, G., Danielson, G. E., Elias, J. H., Lonsdale, C. J., & Rice, W. L. 1987, *ApJ*, 320, 238
- Solomon, P.M., Downes, D., Radford, S.J.E., & Barrett, J.W. 1997, *ApJ*, 487, 144
- Surace, J., Sanders, D. B., Vacca, W. D., Veilleux, S., & Mazzarella, J. M. 1998, *ApJ*, 492, 116
- van Breugel, W. 2000, “Proceedings on Ultraluminous Galaxies: Monsters or Babies”, (Kluwer: Germany), eds. L. Tacconi and D. Lutz, in press

Fig. 1.— A plot of F_ν at 1.4 GHz against F_ν at $60\mu\text{m}$ showing all matches of the positional cross-correlation of FIRST with the *IRAS* FSC (the open triangles), along with several comparison samples taken from the literature. The well-known radio–FIR correlation for star-forming galaxies extends to the faintest flux limits probed by the FF objects.

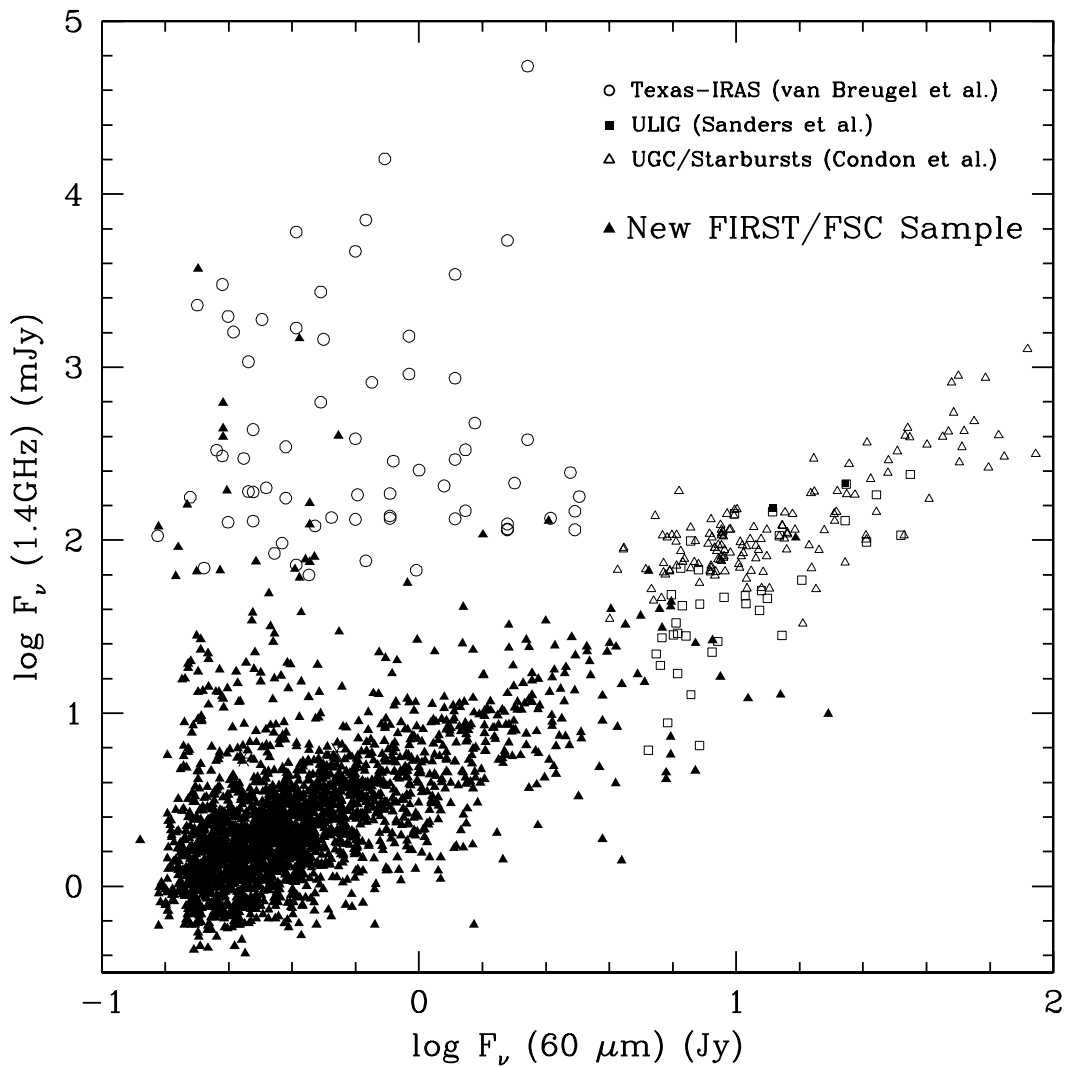


Fig. 2.— Spectra of four objects from Table 1 which cover the range in redshift, spectral type, and signal to noise of the sample.

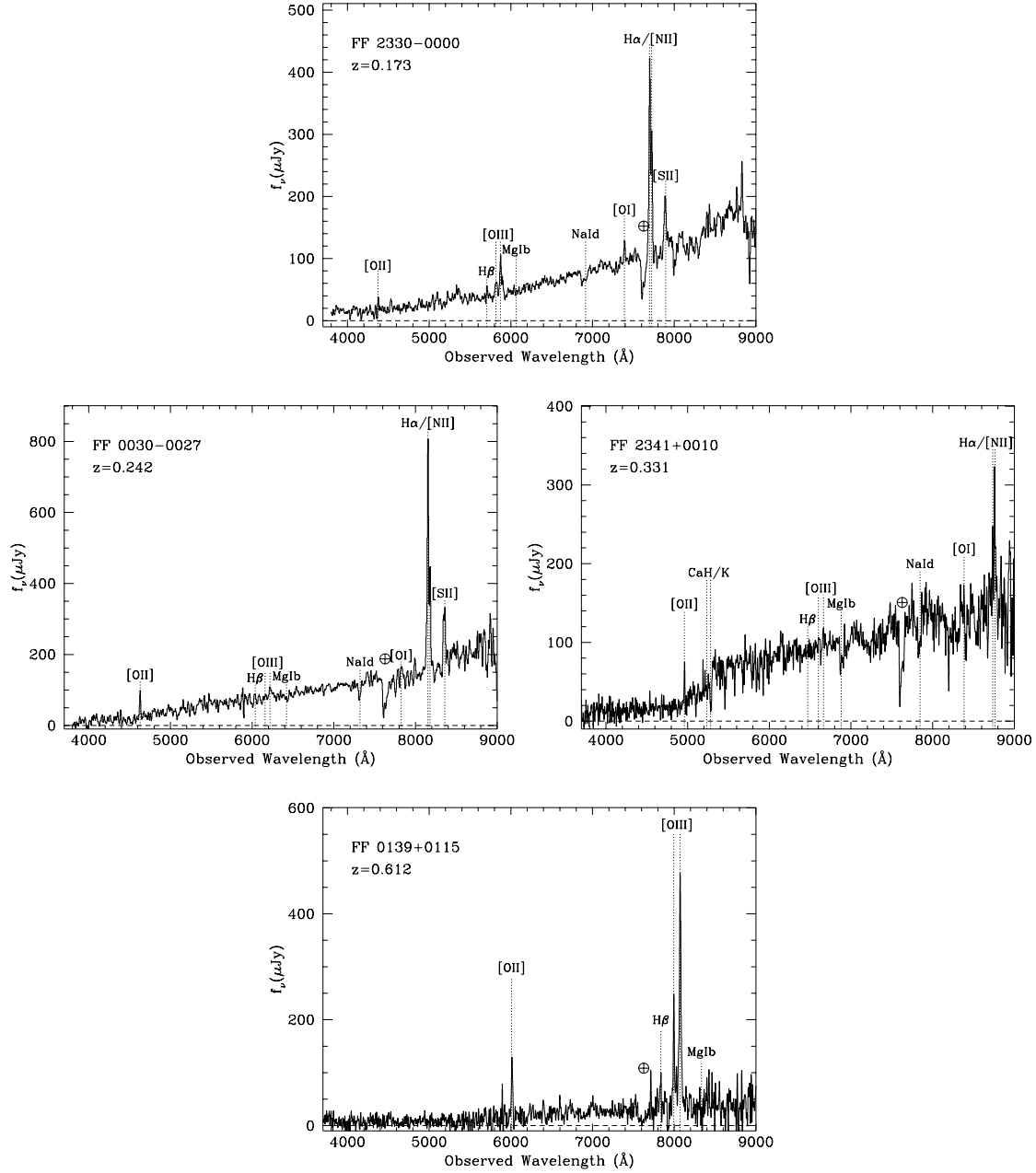


Fig. 3.— (a-bb) For each of the FF objects in Table 1 we show on the left the DSS finding chart centered on the FIRST radio position, which is marked by a small circle of diameter 5 arcsec, with the FSC 95% confidence limit error ellipse superposed. The astrometric uncertainty between the optical and radio reference frames is ~ 1 arcsec. On the right in each panel is a closeup view of the K -band image of the identified source. North is up and East to the left in all panels.

Fig. 4.— A plot of the $\log P_{1.4\text{GHz}}$ against $\log L_{\text{FIR}}$ showing our new FF sample as solid triangles, along with several comparison samples taken from the literature. Three well-known ULIG are marked by name. Radio-loud quasars and BL Lacs are included at the most luminous end of the track traced by the Texas-FSC sources. The luminosities for F10214 have been corrected for gravitational lensing.

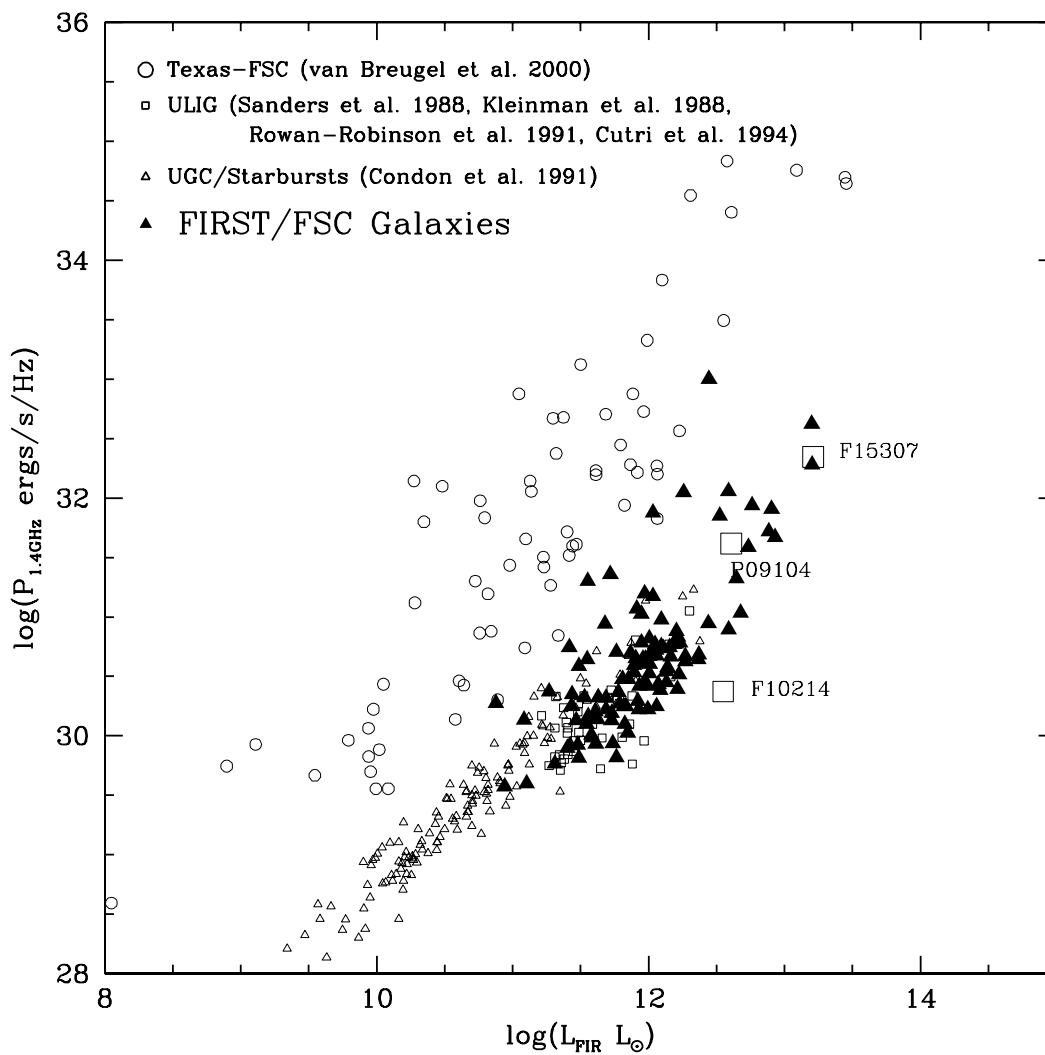
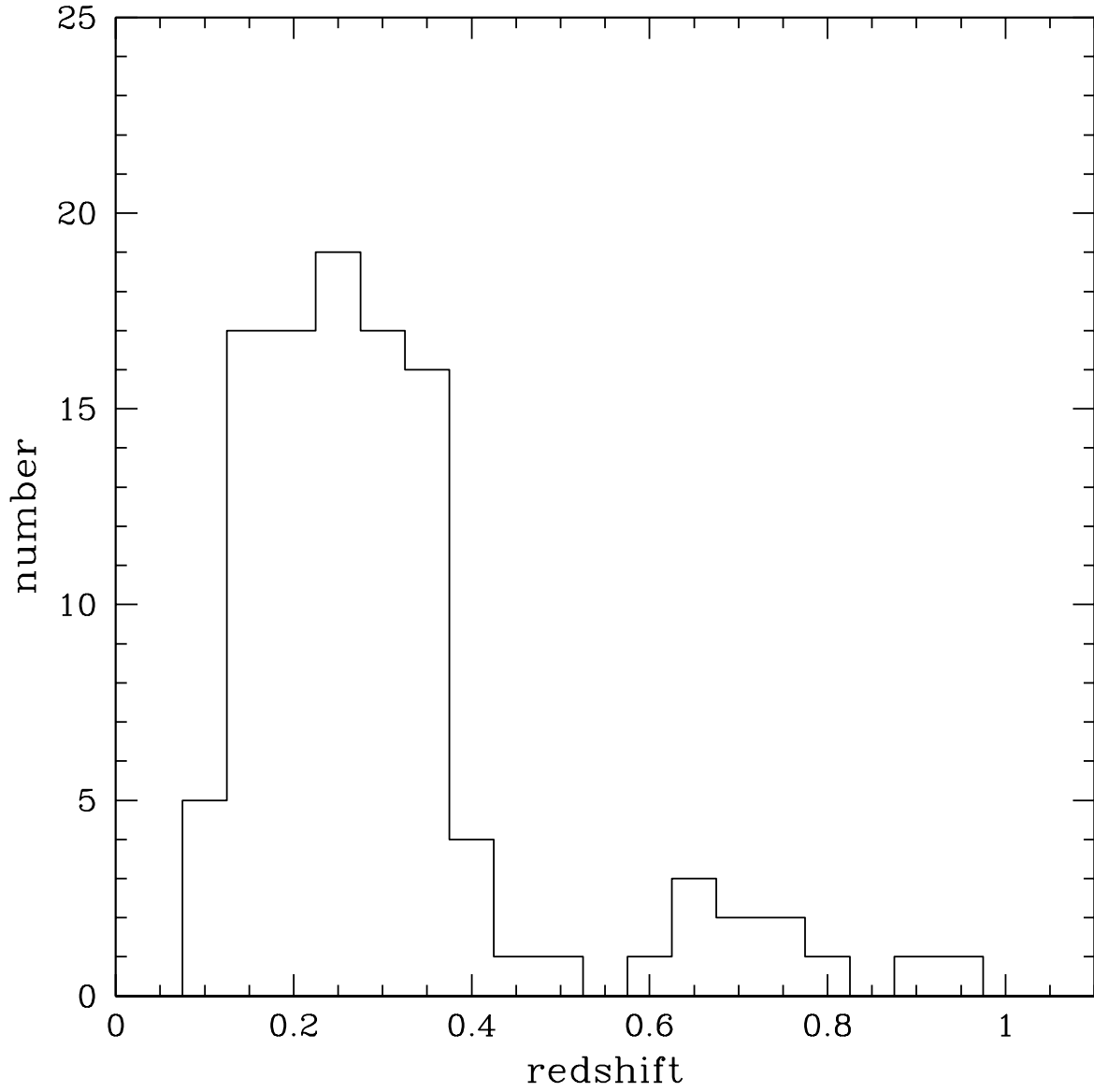


Fig. 5.— A redshift histogram of the identified FF targets.



This figure "f3a.gif" is available in "gif" format from:

<http://arxiv.org/ps/astro-ph/0006003v1>

This figure "f3aa.gif" is available in "gif" format from:

<http://arxiv.org/ps/astro-ph/0006003v1>

This figure "f3ab.gif" is available in "gif" format from:

<http://arxiv.org/ps/astro-ph/0006003v1>

This figure "f3ac.gif" is available in "gif" format from:

<http://arxiv.org/ps/astro-ph/0006003v1>

This figure "f3ad.gif" is available in "gif" format from:

<http://arxiv.org/ps/astro-ph/0006003v1>

This figure "f3ae.gif" is available in "gif" format from:

<http://arxiv.org/ps/astro-ph/0006003v1>

This figure "f3af.gif" is available in "gif" format from:

<http://arxiv.org/ps/astro-ph/0006003v1>

This figure "f3ag.gif" is available in "gif" format from:

<http://arxiv.org/ps/astro-ph/0006003v1>

This figure "f3ah.gif" is available in "gif" format from:

<http://arxiv.org/ps/astro-ph/0006003v1>

This figure "f3ai.gif" is available in "gif" format from:

<http://arxiv.org/ps/astro-ph/0006003v1>

This figure "f3aj.gif" is available in "gif" format from:

<http://arxiv.org/ps/astro-ph/0006003v1>

This figure "f3ak.gif" is available in "gif" format from:

<http://arxiv.org/ps/astro-ph/0006003v1>

This figure "f3a1.gif" is available in "gif" format from:

<http://arxiv.org/ps/astro-ph/0006003v1>

This figure "f3am.gif" is available in "gif" format from:

<http://arxiv.org/ps/astro-ph/0006003v1>

This figure "f3an.gif" is available in "gif" format from:

<http://arxiv.org/ps/astro-ph/0006003v1>

This figure "f3ao.gif" is available in "gif" format from:

<http://arxiv.org/ps/astro-ph/0006003v1>

This figure "f3ap.gif" is available in "gif" format from:

<http://arxiv.org/ps/astro-ph/0006003v1>

This figure "f3aq.gif" is available in "gif" format from:

<http://arxiv.org/ps/astro-ph/0006003v1>

This figure "f3ar.gif" is available in "gif" format from:

<http://arxiv.org/ps/astro-ph/0006003v1>

This figure "f3as.gif" is available in "gif" format from:

<http://arxiv.org/ps/astro-ph/0006003v1>

This figure "f3at.gif" is available in "gif" format from:

<http://arxiv.org/ps/astro-ph/0006003v1>

This figure "f3au.gif" is available in "gif" format from:

<http://arxiv.org/ps/astro-ph/0006003v1>

This figure "f3av.gif" is available in "gif" format from:

<http://arxiv.org/ps/astro-ph/0006003v1>

This figure "f3aw.gif" is available in "gif" format from:

<http://arxiv.org/ps/astro-ph/0006003v1>

This figure "f3ax.gif" is available in "gif" format from:

<http://arxiv.org/ps/astro-ph/0006003v1>

This figure "f3ay.gif" is available in "gif" format from:

<http://arxiv.org/ps/astro-ph/0006003v1>

This figure "f3az.gif" is available in "gif" format from:

<http://arxiv.org/ps/astro-ph/0006003v1>

This figure "f3b.gif" is available in "gif" format from:

<http://arxiv.org/ps/astro-ph/0006003v1>

This figure "f3ba.gif" is available in "gif" format from:

<http://arxiv.org/ps/astro-ph/0006003v1>

This figure "f3bb.gif" is available in "gif" format from:

<http://arxiv.org/ps/astro-ph/0006003v1>

This figure "f3c.gif" is available in "gif" format from:

<http://arxiv.org/ps/astro-ph/0006003v1>

This figure "f3d.gif" is available in "gif" format from:

<http://arxiv.org/ps/astro-ph/0006003v1>

This figure "f3e.gif" is available in "gif" format from:

<http://arxiv.org/ps/astro-ph/0006003v1>

This figure "f3f.gif" is available in "gif" format from:

<http://arxiv.org/ps/astro-ph/0006003v1>

This figure "f3g.gif" is available in "gif" format from:

<http://arxiv.org/ps/astro-ph/0006003v1>

This figure "f3h.gif" is available in "gif" format from:

<http://arxiv.org/ps/astro-ph/0006003v1>

This figure "f3i.gif" is available in "gif" format from:

<http://arxiv.org/ps/astro-ph/0006003v1>

This figure "f3j.gif" is available in "gif" format from:

<http://arxiv.org/ps/astro-ph/0006003v1>

This figure "f3k.gif" is available in "gif" format from:

<http://arxiv.org/ps/astro-ph/0006003v1>

This figure "f3l.gif" is available in "gif" format from:

<http://arxiv.org/ps/astro-ph/0006003v1>

This figure "f3m.gif" is available in "gif" format from:

<http://arxiv.org/ps/astro-ph/0006003v1>

This figure "f3n.gif" is available in "gif" format from:

<http://arxiv.org/ps/astro-ph/0006003v1>

This figure "f3o.gif" is available in "gif" format from:

<http://arxiv.org/ps/astro-ph/0006003v1>

This figure "f3p.gif" is available in "gif" format from:

<http://arxiv.org/ps/astro-ph/0006003v1>

This figure "f3q.gif" is available in "gif" format from:

<http://arxiv.org/ps/astro-ph/0006003v1>

This figure "f3r.gif" is available in "gif" format from:

<http://arxiv.org/ps/astro-ph/0006003v1>

This figure "f3s.gif" is available in "gif" format from:

<http://arxiv.org/ps/astro-ph/0006003v1>

This figure "f3t.gif" is available in "gif" format from:

<http://arxiv.org/ps/astro-ph/0006003v1>

This figure "f3u.gif" is available in "gif" format from:

<http://arxiv.org/ps/astro-ph/0006003v1>

This figure "f3v.gif" is available in "gif" format from:

<http://arxiv.org/ps/astro-ph/0006003v1>

This figure "f3w.gif" is available in "gif" format from:

<http://arxiv.org/ps/astro-ph/0006003v1>

This figure "f3x.gif" is available in "gif" format from:

<http://arxiv.org/ps/astro-ph/0006003v1>

This figure "f3y.gif" is available in "gif" format from:

<http://arxiv.org/ps/astro-ph/0006003v1>

This figure "f3z.gif" is available in "gif" format from:

<http://arxiv.org/ps/astro-ph/0006003v1>

TABLE 1. FIRST/FSC Sample

Source	FSC	RA J2000	Dec. J2000	z	K ^a mag	S _{60μm} Jy	S _{100μm} Jy	log L_{FIR} L_{\odot}	S _{1.4 GHz} mJy	20 cm morphology	K -band morphology
FF 0001-0141	Z23592-0157	00 01 45.162	-01 41 37.06	0.278	15.6	0.16	(0.24) ^b	11.73	10.1	2 lobes	two nuclei
FF 0010+0042	Z00076+0025	00 10 17.529	+00 42 44.77	0.320	16.0	0.23	0.39	12.04	4.87	complex	multiple nuclei
FF 0011-0038	F00090-0054	00 11 38.852	-00 38 13.16	0.195	15.9	0.46	(0.61)	11.83	1.17	extended	two nuclei
FF 0013-0123	F00104-0139	00 13 03.749	-01 23 05.06	0.162	16.0	0.72	0.71	11.81	4.12	extended	normal disk
FF 0029-0009	Z00269-0025	00 29 29.530	-00 09 11.45	0.168	14.6	0.22	0.41	11.43	1.06	extended	normal
FF 0030-0027	F00275-0044	00 30 09.099	-00 27 44.40	0.242	14.5	0.63	1.52	12.28	2.52	point	normal & companion
FF 0050-0039	F00476-0054	00 50 09.806	-00 39 00.96	0.727	16.8	0.26	0.44	12.92	4.32	extended	tail & companion
FF 0053+0056	F00507+0040	00 53 19.971	+00 56 39.69	0.235	15.8	0.58	(0.71)	12.09	1.53	point	disturbed spiral
FF 0111-0123	Z01092-0139	01 11 46.946	-01 23 17.85	0.154	14.8	0.35	0.44	11.48	1.28	point	normal disk
FF 0123+0114	Z01205+0058	01 23 06.973	+01 14 10.03	0.089	19.8	0.26	0.55	10.94	1.78	double	disturbed
FF 0138+0031	F01360+0016	01 38 38.880	+00 31 49.77	0.148	15.2	0.42	0.66	11.56	2.42	point	normal
FF 0139+0115	Z01368+0100	01 39 27.181	+01 15 47.17	0.612	16.8	0.23	0.21	12.60	9.01	complex	tail
FF 0146+0136	F01436+0120	01 46 13.345	+01 36 01.17	0.230	14.8	0.18	0.21	11.56	13.2	point	normal
FF 0148+0029	F01462+0014	01 48 52.602	+00 29 00.06	0.279	15.4	0.35	0.68	12.11	2.38	point	interacting pair
FF 0234-0139	Z02317-0152	02 34 21.905	-01 39 00.71	0.645	17.8	0.14	(0.15)	12.46	70.3	extended	faint w/ companions
FF 0236+0051	Z02339+0038	02 36 35.065	+00 51 27.08	0.207	14.3	0.15	0.23	11.42	4.58	point	disturbed
FF 0238-0033	Z02354-0046	02 38 01.464	-00 33 42.29	0.56:	14.9	0.19	(0.33)	12.10	2.28	extended	merger
FF 0240-0042	Z02376-0054	02 40 08.576	-00 42 03.56	0.41:	16.1	0.21	0.68	12.38	0.84	multiple	normal w/ companions
FF 0244-0030	F02417-0043	02 44 17.440	-00 30 40.95	0.200	14.3	0.47	1.04	11.95	9.39	extended	interacting pair
FF 0245+0123	Z02433+0110	02 45 55.355	+01 23 28.40	0.798	17.5	0.21	0.40	12.95	2.03	extended	disturbed disk
FF 0252-0120	Z02503-0132	02 52 55.473	-01 20 19.97	0.20:	16.6	0.18	0.32	11.49	0.58	point	normal
FF 0253-0046	F02513-0058	02 53 53.940	-00 46 15.48	0.182	15.3	0.22	0.75	11.64	2.25	extended	normal w/ companion
FF 0303-0202	Z03009-0213	03 03 26.877	-02 02 09.58	0.118	14.1	0.22	0.38	11.09	3.62	extended	normal disk
FF 0307-0019	F03048-0030	03 07 25.020	-00 19 00.70	0.269	13.8	0.41	0.20	11.98	7.46	extended	normal
FF 0312+0058	F03100+0047	03 12 38.445	+00 58 33.86	0.130	14.3	0.29	0.97	11.43	3.84	extended	disturbed
FF 0317-0208	Z03150-0219	03 17 33.301	-02 08 47.54	0.319	15.8	0.17	0.60	12.06	1.72	extended	interacting
FF 0317-0129	Z03151-0140	03 17 43.635	-01 29 07.33	0.265	15.0	0.23	0.49	11.90	1.67	point	two nuclei
FF 0317-0054	Z03153-0105	03 17 52.931	-00 54 17.44	0.117	14.9	0.17	(0.16)	10.88	5.11	extended	normal
FF 0738+2856	F07353+2903	07 38 29.856	+28 56 38.74	0.334	15.8	0.25	0.56	12.17	1.38	extended	interacting pair
FF 0748+3343	F07449+3350	07 48 10.591	+33 43 27.13	0.356	15.6	0.61	1.22	12.60	2.03	point	disturbed disk
FF 0758+2851	F07556+2859	07 58 45.956	+28 51 32.76	0.126	14.9	0.66	1.06	11.61	3.72	point	interacting
FF 0800+3126	F07575+3133	08 00 40.366	+31 25 39.47	0.36:	15.6	0.20	0.55	12.19	1.49	extended	interacting pair
FF 0802+3030	F07590+3038	08 02 11.531	+30 30 25.09	0.14:	15.6	0.26	0.41	11.31	1.06	extended	normal w/ companion
FF 0804+3919	F08007+3928	08 04 07.399	+39 19 27.63	0.164	14.4	0.30	0.60	11.55	5.90	point	normal
FF 0814+3030	F08112+3039	08 14 20.798	+30 30 50.53	0.124	14.6	0.32	0.48	11.27	5.64	point	normal
FF 0816+3101	F08136+3110	08 16 45.730	+31 01 19.90	0.407	15.9	0.22	0.28	12.21	1.16	point	two nuclei
FF 0817+3125	F08143+3134	08 17 26.652	+31 25 10.59	0.359	15.9	0.22	(0.15)	12.01	1.68	point	disturbed
FF 0822+3726	F08195+3736	08 22 50.177	+37 26 58.16	0.263	15.7	0.18	0.38	11.78	1.16	complex	interacting pair
FF 0823+3202	F08208+3211	08 23 54.616	+32 02 12.03	0.396	16.3	0.24	0.44	12.28	0.97	point	disturbed
FF 0826+3042	F08231+3052	08 26 11.644	+30 42 44.17	0.248	15.0	0.39	0.97	12.10	3.19	point	normal

TABLE 1. (continued)

Source	FSC	RA J2000	Dec. J2000	z	K ^a mag	$S_{60\mu m}$ Jy	$S_{100\mu m}$ Jy	$\log L_{FIR}$ L_{\odot}	$S_{1.4\text{ GHz}}$ mJy	20 cm morphology	K-band morphology
FF 0835+3257	F08322+3307	08 35 22.086	+32 57 10.96	0.288	15.3	0.30	0.32	11.98	1.82	extended	disturbed disk
FF 0835+3559	F08322+3609	08 35 27.440	+35 59 33.07	0.201	15.5	0.38	0.63	11.85	0.85	point	normal
FF 0852+3502	F08498+3513	08 52 55.563	+35 02 10.39	0.190	14.6	0.18	0.41	11.49	3.83	extended	tidal tail
FF 0855+3708	F08526+3720	08 55 54.451	+37 08 59.83	0.357	15.4	0.24	0.35	12.14	0.90	point	double nuclei
FF 0856+3450	F08532+3502	08 56 24.852	+34 50 24.82	0.220	14.9	0.31	0.90	11.92	8.51	point	disturbed disk
FF 0858+3925	F08551+3550	08 58 14.498	+39 25 45.05	0.228	16.2	0.26	0.26	11.69	1.12	point	normal
FF 0903+3630	F09008+3643	09 03 59.927	+36 30 54.99	0.289	14.9	0.29	0.45	12.03	2.05	extended	normal
FF 0907+3931	F09045+3943	09 07 42.264	+39 31 49.47	0.224	15.4	0.28	0.64	11.84	1.24	point	normal
FF 0937+3857	F09346+3911	09 37 41.664	+38 57 52.60	0.621	16.5	0.22	0.32	12.69	0.77	point	disturbed, tails
FF 0944+3100	F09415+3114	09 44 30.265	+31 00 20.81	0.261	15.5	0.28	0.43	11.91	2.28	extended	pair
FF 0945+2939	F09429+2952	09 45 50.982	+29 39 08.40	0.274	15.5	0.37	0.52	12.07	0.81	point	tidal tail?
FF 0947+4025	F09443+4039	09 47 29.313	+40 25 15.13	0.219	16.0	0.43	0.27	11.82	1.30	point	disturbed
FF 0959+4105	F09567+4119	09 59 50.161	+41 05 04.60	0.361	15.4	0.22	0.54	12.21	1.56	extended	normal w /companion
FF 1002+3404	F09593+3418	10 02 14.621	+34 04 17.25	0.279	15.4	0.21	0.58	11.96	1.95	extended	interacting
FF 1004+3957	F10017+4011	10 04 45.159	+39 57 31.85	0.31:	16.6	0.26	0.31	12.01	1.61	extended	disturbed
FF 1016+3951	F10131+4006	10 16 08.616	+39 51 20.46	0.307	15.4	0.25	0.47	12.05	2.10	complex	tidal tail, shells?
FF 1017+2823	F10150+2838	10 17 51.833	+28 23 15.04	0.256	15.2	0.16	0.50	11.79	0.98	extended	disturbed
FF 1018+3649	F10156+3705	10 18 34.539	+36 49 51.75	0.490	16.6	0.23	0.57	12.53	9.18	extended	disturbed
FF 1025+4129	F10228+4145	10 25 52.932	+41 29 41.68	0.309	16.8	0.27	0.47	12.08	0.96	extended	normal w/ companions
FF 1032+3453	F10300+3509	10 32 53.897	+34 53 59.03	0.255	15.4	0.26	0.74	11.98	1.50	double	two nuclei
FF 1042+3231	F10398+3247	10 42 40.815	+32 31 30.99	0.633	17.4	0.22	0.54	12.78	6.34	point	interacting pair
FF 1051+3711	F10485+3726	10 51 18.496	+37 10 43.43	0.356	16.6	0.18	(0.31)	12.04	19.5	point	disturbed, fan
FF 1053+3150	F10509+3206	10 53 46.352	+31 49 52.15	0.357	15.9	0.24	0.40	12.16	1.43	extended	normal w/ companion
FF 1106+3201	F11038+3217	11 06 35.716	+32 01 46.39	0.90:	18.2 ^c	0.23	0.70	13.22	13.7	extended	normal w/ companions
FF 1115+3045	F11130+3102	11 15 42.109	+30 45 37.60	0.152	14.5	0.27	0.65	11.47	2.13	extended	normal w/ companion
FF 1124+3836	F11215+3853	11 24 14.557	+38 36 50.55	0.294	16.2	0.14	0.45	11.87	1.94	point	normal
FF 1200+3004	F11582+3020	12 00 46.812	+30 04 14.82	0.224	15.1	1.23	1.52	12.38	3.38	extended	disturbed
FF 1223+3339	F12205+3356	12 23 00.312	+33 39 28.86	0.263	15.0	0.62	0.80	12.24	3.01	extended	interacting
FF 1230+3523	F12278+3539	12 30 17.847	+35 23 05.17	0.336	16.3	0.27	0.64	12.22	0.73	point	disturbed
FF 1242+2905	F12401+2921	12 42 32.497	+29 05 14.75	0.260	17.2	0.20	0.72	11.94	1.34	extended	normal
FF 1245+3509	F12431+3526	12 45 33.503	+35 09 52.76	0.219	15.7	0.30	0.44	11.77	3.70	extended	normal
FF 1250+3649	F12479+3705	12 50 18.181	+36 49 14.04	0.279	14.9	0.29	0.47	12.00	1.15	point	spiral
FF 1251+3211	F12494+3227	12 51 54.952	+32 11 10.59	0.326:	15.9	0.22	0.61	12.15	1.16	point	tidal tail
FF 1412+3014	F14102+3027	14 12 24.952	+30 14 09.78	0.257	15.4	0.19	0.67	11.90	2.06	point	faint tail
FF 1421+3726	F14198+3740	14 21 54.911	+37 26 18.76	0.291	15.1	0.20	0.63	12.01	1.34	extended	normal w/ companion
FF 1429+3957	F14277+4010	14 29 42.332	+39 57 42.88	0.388	16.3	0.25	0.31	12.21	1.65	point	normal
FF 1449+3436	F14478+3448	14 49 49.394	+34 36 31.77	0.160	15.1	0.22	0.47	11.41	1.12	extended	normal
FF 1453+3839	F14516+3851	14 53 35.964	+38 39 13.10	0.152	15.3	0.50	0.58	11.62	1.35	point	normal, tail?
FF 1456+3337	F14548+3349	14 56 58.427	+33 37 09.98	0.443	16.2	0.23	0.62	12.45	1.43	point	two nuclei

TABLE 1. (continued)

Source	FSC	RA J2000	Dec. J2000	z	K ^a mag	S _{60μm} Jy	S _{100μm} Jy	log L_{FIR} L_{\odot}	S _{1.4 GHz} mJy	20 cm morphology	K-band morphology
FF 1505+3026	F15034+3037	15 05 33.036	+30 26 21.35	0.217	14.8	0.20	0.23	11.55	0.94	point	three nuclei
FF 1514+3629	F15126+3640	15 14 33.118	+36 29 42.36	0.338	16.4	0.24	0.48	12.14	0.82	point	interacting pair
FF 1520+3013	F15182+3023	15 20 16.831	+30 12 58.63	0.254	16.0	0.35	0.60	12.00	0.89	multiple	interacting triple?
FF 1532+3242	F15307+3252	15 32 44.052	+32 42 46.73	0.926	16.4	0.28	0.50	13.22	5.89	extended	interacting pair
FF 1540+3758	F15386+3807	15 40 31.050	+37 58 14.53	0.183	14.6	0.20	0.47	11.60	1.05	double?	interacting pair
FF 1551+3445	F15492+3454	15 51 08.864	+34 45 33.59	0.312	16.2	0.30	(0.21)	12.02	1.39	extended	merger
FF 1614+3234	F16124+3241	16 14 22.105	+32 34 03.66	0.710	16.6 ^c	0.17	(0.21)	12.66	1.19	point	tidal tail
FF 1615+2912	F16134+2919	16 15 27.963	+29 12 00.20	0.168	15.5	0.30	0.79	11.63	1.75	point	normal
FF 1652+3816	F16508+3821	16 52 36.207	+38 16 27.65	0.147	14.7	0.42	0.78	11.58	1.72	point	normal w/ companions
FF 1659+3549	F16576+3553	16 59 24.669	+35 49 01.74	0.371	17.0	0.22	0.53	12.25	0.79	point	disturbed w/ companion
FF 1707+3725	F17054+3729	17 07 11.795	+37 25 55.32	0.311	15.8	0.18	0.40	11.96	2.11	extended	normal
FF 1713+3843	F17120+3846	17 13 46.085	+38 43 04.77	0.171	15.3	0.38	0.92	11.73	1.66	extended	interacting pair
FF 1725+3709	F17233+3712	17 25 07.401	+37 09 32.09	0.689	17.9	0.24	0.23	12.75	2.33	point	faint, interacting?
FF 1726+3656	F17252+3659	17 26 57.757	+36 56 39.45	0.365	16.0	0.30	0.35	12.23	1.67	double?	disturbed
FF 2119+0007	Z21169-0005	21 19 32.215	+00 07 44.43	0.289	14.8	0.15	0.16	11.69	3.55	point	interacting pair
FF 2122-0000	F21198-0013	21 22 20.646	-00 00 46.41	0.297	15.4	0.19	(0.41)	11.93	0.75	point	tidal tail
FF 2131-0141	Z21293-0154	21 31 53.490	-01 41 43.35	0.730	19:	0.19	0.56	12.90	2.79	complex	faint
FF 2136-0112	F21340-0125	21 36 34.229	-01 12 08.38	0.21:	16.2	0.33	1.12	11.95	3.20	point	normal w/ companion
FF 2136-0019	F21341-0033	21 36 46.011	-00 19 47.06	0.210	15.6	0.32	(0.40)	11.73	1.24	extended	two nuclei
FF 2200-0038	F21581-0053	22 00 47.250	-00 38 48.08	0.356	16.1	0.35	(0.40)	12.27	28.9	extended	tidal tails
FF 2200+0108	Z21583+0054	22 00 51.859	+01 08 27.08	0.164	14.7	0.23	0.72	11.53	2.82	extended	normal w/ companion
FF 2216+0058	F22134+0043	22 16 02.721	+00 58 10.65	0.212	16.5	0.46	0.72	11.93	1.31	point	asymmetric
FF 2221-0042	Z22188-0058	22 21 26.066	-00 42 39.08	0.189	17.3	0.26	1.00	11.77	0.66	point	faint
FF 2330-0025	F23279-0041	23 30 34.920	-00 25 03.98	0.252	15.8	0.19	0.62	11.86	1.65	extended	tidal tails
FF 2331-0000	Z23283-0017	23 30 54.903	-00 00 40.12	0.173	15.3	0.16	(0.54)	11.44	2.68	extended	disturbed w/ companion
FF 2331-0143	Z23292-0159	23 31 50.519	-01 43 05.97	0.228	14.9	0.20	0.42	11.69	1.40	extended	interacting
FF 2341-0201	F23390-0217	23 41 36.151	-02 01 06.44	0.174	15.9	0.32	0.57	11.59	1.20	point	interacting
FF 2341+0016	F23392+0000	23 41 48.137	+00 16 55.06	0.331	16.0	0.23	0.38	12.07	1.43	extended	interacting
FF 2352-0015	Z23503-0032	23 52 53.171	-00 15 24.69	0.227	15.3	0.19	0.57	11.74	0.59	point	interacting

^aK-band magnitudes were measured through a 3.0 arcsec diameter aperture.^b100 μ m fluxes shown in parentheses are upper limits.^cK-band data obtained with NIRC at Keck I